Energy States in $LaAlO_3/SrTiO_3$ Quantum Wells

University of Texas at Austin

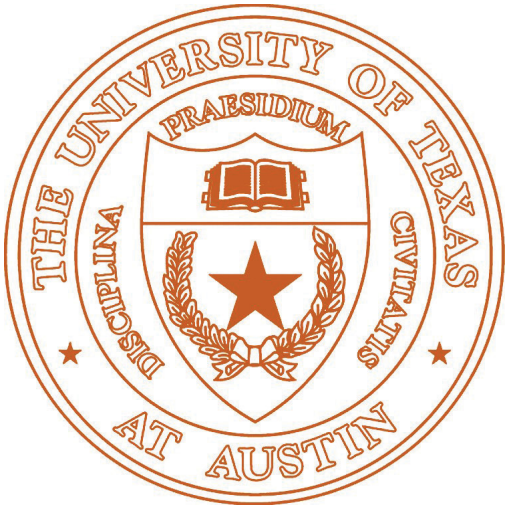

Matthew Butcher

May 8, 2015

Abstract

In this work, we study the energy states and transitions in $LaAlO_3/SrTiO_3$ heterostructures. Using a computational Schrödinger - Poisson solver to find the confined energy states and Fermi theory to determine the occupation of those states, we can begin to describe the available energy transitions stimulated by photon absorption and emission. Using a finite difference approach, we find the energy states approximately to within 10% of the true values for arbitrary finite well potentials. Additionally, we can engineer well structures to have transitions at a desired energy in the infrared region with high enough absorption coefficients to be seen experimentally. In the future, this code will continue to be used to inform experimental studies of $LaAlO_3/SrTiO_3$ quantum wells for applications in infrared sensing.

Contents

Chapter 1

Background

1.0 Note on units

For the entirety of this thesis and for the work it outlines I have used pseudo-CGS units, mainly just choosing convenient units and adapting the equations to give the correct values. All of the distances are in Angstroms (Å) and energies in electron volts (eV). In this system, some physical constants are as follows:

$e = 1$	The charge of an electron
$\epsilon_0 = 1$	The permittivity of free space
$\frac{\hbar^2}{2m_0} \approx 3.81 \text{ eV} \cdot \text{Å}^2$	Electron kinetic energy constant

1.1 Introduction

1.1.1 Quantum Wells

Many modern technological devices can attribute their functionality to their molecular makeup. In a solid, the ways electrons interact with the atomic nuclei and with each other determine many useful properties of the material. So, a fundamental understanding of electronic structure in various materials is the key to creating new technologies. One interesting way to influence the electronic structure of a material is to use two materials and put them

together, as in Figure 1.1. This general type of structure (where two or more materials are layered together) is called a heterostructure and this specific "sandwich"-type material is called a quantum well [1]. When the quantum

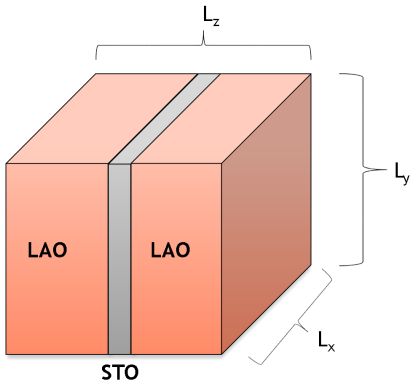

Figure 1.1: A schematic drawing of a quantum well heterostructure. Here LAO is $LaAlO_3$ and STO is $SrTiO_3$. The electrons are confined to the STO layer because LAO's conduction band has a higher energy floor.

well is thin enough (on the order of 1 to 100 atoms, or 5 to 500 Å), the allowed energy levels that are normally continuous in a macroscopic solid become discrete energy levels, governed by the Schrödinger Equation. So, these structures provide a simpler way to control and calculate the available electron energy states. By building more complex layered heterostructures from this basic quantum well, we can create many devices for many types of optical and electronic applications.

1.1.2 The LAO/STO Quantum Well

This research focuses on the $LaAlO_3$ (LAO) / $SrTiO_3$ (STO) quantum well because the interface between the two materials has some interesting and desirable properties. As metal oxides, both LAO and STO are normally insulators. However, when placed together in a heterostructure their interface becomes metallic in the sense that the electrons can then move freely within the plane of the interface [2]. In addition, the relatively large bandgap of 5.6 eV in LAO [3] allows more opportunity to tune a quantum well device to specific energies within a given range.

1.1.3 Applications for Quantum Wells

Some interesting possible applications of the structures studied in this research include quantum cascade lasers and terahertz devices.

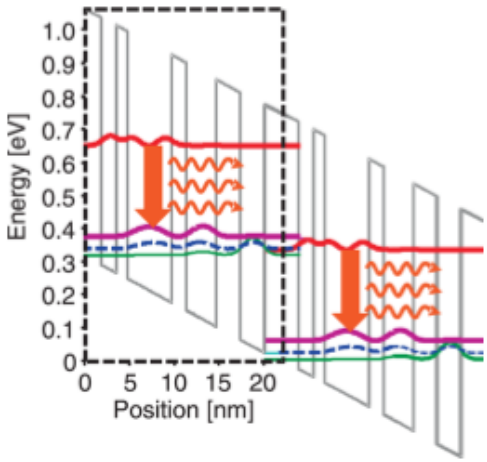

Figure 1.2: A schematic drawing of a quantum cascade laser heterostructure. The upper laser level is the red state, and the lower laser level is the purple state. After falling from the upper level to the lower level and emitting a photon, the electron relaxes down by phonon scattering until it can move into the next upper laser state. Reproduced from [4] with permission from the American Institute of Physics.

A quantum cascade laser can be made from a periodic multiple quantum well (MQW) structure as in Figure 1.2. Within each period, there are energy states for injection, depletion, and two laser levels. An electron in the upper laser level relaxes down to the lower laser level to emit photons of a specific desired energy. Then, the electron falls into the depletion state and then to the injector state. A voltage can be applied across the periods in the structure in such a way as to nearly match the injector state of one period with the upper laser level of the next period. Thus, an electron can travel through multiple periods, emitting multiple photons (all of a single energy) along the way [4].

Another interesting use for quantum wells is the creation of terahertz devices. Devices in the $1 - 10$ THz region of the electromagnetic spectrum have become popular research topics in recent years because they bridge the gap between microwave and infrared where not many devices currently operate. This region is important for sensing and communications [5]. A terahertz sensing device could be used for imaging studies of many biological molecules, or for studying semiconductor properties. Additionally, as the electromagnetic spectrum becomes more and more saturated in communication technologies, it will be important to be able to reach a wider range of frequencies. Quantum well devices can be used to reach these frequencies because their energy transitions can change based on their size.

1.2 Theory

1.2.1 General Construction and Quantum Mechanics of Solids

Lattices

The quantum mechanics of solids take place in the framework of the Bravais lattice [6]. In a Bravais lattice, the neighborhood around any specific point in the lattice is exactly the same as the one around any other point. In other words, the lattice is invariant with respect to translation by a lattice vector. A point on a 3-dimensional Bravais lattice is defined as

$$\vec{R} \equiv n_1\vec{a}_1 + n_2\vec{a}_2 + n_3\vec{a}_3; \quad n_i \in \mathbb{Z} \tag{1.1}$$

The $\vec{a}_i$ are known as primitive vectors, and must be linearly independent. A given lattice has an infinite number of possible choices for primitive vectors, but they are chosen to be most convenient for a given calculation.

Lattice Structure of LAO and STO

LAO and STO are both perovskites, a subclass of metal oxides obeying the general formula ABO_3. A diagram of a perovskite unit cell is shown in Figure 1.3. The length of the cells in LAO and STO are slightly different; however, they deform to approximately the same value when synthesized in a heterostructure. This distance is taken to be 3.9 Å in this work.

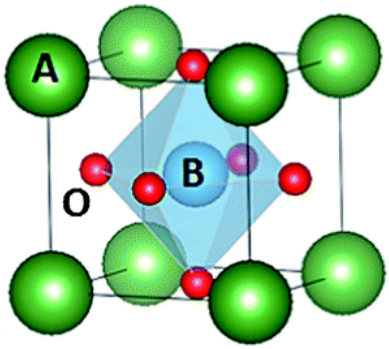

Figure 1.3: The perovskite unit cell. Here A is Sr or La and B is Ti or Al in STO and LAO, respectively. Reproduced from [7] with permission from The Royal Society of Chemistry.

Schrödinger Equation and the Free Electron Fermi Gas

All quantum mechanical particles obey the Schrödinger equation, and electrons in solids are no exception:

$$\begin{aligned} \hat{H}\Psi &= E\Psi \\ \hat{H} &= -\frac{\hbar^2}{2m_0}\sum_{l=1}^{N}\nabla_l^2 + U(\vec{r}) \end{aligned} \tag{1.2}$$

where m_0 is the mass of an electron, $\hbar$ is Planck's reduced constant, and $\nabla^2 = \left(\frac{\partial^2}{\partial x^2} + \frac{\partial^2}{\partial y^2} + \frac{\partial^2}{\partial z^2}\right)$.
The key is using a potential energy function $U(\vec{r})$ that is both accurate and solvable. For a first approximation, however, we will only consider the case of a single electron moving in a conduction band so that it sees no potential from positive ions or other electrons. The total wavefunction Ψ will in this case be a product of single electron wavefunctions ψ_l. So, Equation 1.2 becomes

$$\hat{H}\psi_l(x,y,z) = -\frac{\hbar^2}{2m_0}\nabla_l^2\psi_l(x,y,z) = E_l\,\psi_l(x,y,z) \tag{1.3}$$

Now, we will consider a cube of dimension L and impose the following periodic boundary conditions:

$$\Psi(x+L,y,z) = \Psi(x,y+L,z) = \Psi(x,y,z+L) = \Psi(x,y,z) \tag{1.4}$$

The physical reason to impose these conditions is not necessarily immediately evident, but will give us verifiable solutions. Solutions to 1.3 under the conditions given in 1.4 will then be

$$\psi_{\vec{k}} = \frac{1}{\sqrt{L^3}} e^{i(k_x x + k_y y + k_z z)} \tag{1.5}$$

with

$$\vec{k} = \frac{2\pi}{L}(n_x, n_y, n_z); \quad n_i \in \mathbb{Z} \tag{1.6}$$

Solutions of this form ensure the boundary conditions 1.4 are met, and the factor $\frac{1}{\sqrt{L^3}}$ ensures that the wavefunction is properly normalized. Now, these solutions define for us the energy of a free electron:

$$E^0_{\vec{k}} = \frac{\hbar^2}{2m_0} |\vec{k}|^2 \tag{1.7}$$

Solutions to the Schrödinger Equation for Quantum Wells

For a quantum well whose walls have infinite height, Equation 1.5 gives the general solution for three dimensions. However, what if the well has finite height? We are interested in electrons that are confined by the well. These energy levels are called bound states, and they are defined as the states whose energies are lower than the height of the well; in other words, these electrons don't have enough energy to "escape" from the well. So, define:

$$\begin{aligned} k &= \sqrt{\frac{2m_0 E}{\hbar^2}} \\ \kappa &= \sqrt{\frac{2m_0(V_0 - E)}{\hbar^2}} \end{aligned} \tag{1.8}$$

Then for the Schrödinger Equation in one dimension with a finite well potential of width $L = z_2 - z_1$,

$$\left[-\frac{\hbar^2}{2m_0} \frac{d^2}{dz^2} + V_(z) \right] \phi(z) = E_z \phi(z) \tag{1.9}$$

$$V(z) = \begin{cases} 0 & z_1 < z < z_2 \\ V_0 & \text{all other } z \end{cases} \tag{1.10}$$

The solutions to the finite well potential are piecewise functions:

$$\phi(z) = \begin{cases} Ae^{\kappa z} & z \leq z_1 \\ B\sin(kz) + C\cos(kz) & z_1 \leq z \leq z_2 \\ De^{-\kappa z} & z \geq z_2 \end{cases} \tag{1.11}$$

Using the conditions that ϕ and $\frac{\partial \phi}{\partial z}$ are continuous at z_1 and z_2, we can do some algebra to obtain the condition on k and κ for the allowed energy states:

$$\cos(kL) + \frac{\kappa^2 - k^2}{k\kappa}\sin(kL) = 0 \tag{1.12}$$

This condition will only give bound states ($E < V_0$), but these are the ones we are truly interested in studying.

Density of States

The Pauli Exclusion Principle allows only two electrons for each wavevector $\vec{k}$: one spin up and one spin down. So, in this way we can begin to talk about the energy distribution for many electrons occupying the various allowed energy states. There are two densities of states, one labeled $D_{\vec{k}}$ and the other labeled $D(E)$. These will represent the number of states available per volume per wavevector $\vec{k}$ and the number of states available per volume per unit energy, respectively. For this work, only the densities of states in two dimensional systems will be needed. The density of $\vec{k}$ states is the reciprocal of the area of one $\vec{k}$ state, divided by volume, times 2 for the two allowed spin states.

$$D_{\vec{k},2D} = 2 \cdot \frac{1}{(\frac{2\pi}{L})^2} \cdot \frac{1}{L^2}$$

$$D_{\vec{k},2D} = \frac{1}{2\pi^2} \tag{1.13}$$

The density of energy states is then defined as

$$D(E) \equiv \int d\vec{k}\, D_{\vec{k}}\, \delta(E - E^0_{\vec{k}}) \tag{1.14}$$

To evaluate the integral in equation 1.14 using the properties of the Dirac delta, we must change the integration variable to energy. To further simplify

the integral, we can exploit the symmetry of the energy function and change to polar coordinates in k:

$$D_{2D}(E) = 2\pi \int_0^\infty dk\, k\, D_{\vec{k}}\, \delta(E - E^0_{\vec{k}}) \tag{1.15}$$

$$= \frac{1}{\pi} \int_0^\infty \frac{dE^0_{\vec{k}}}{|dE^0_{\vec{k}}/dk|} k\, \delta(E - E^0_{\vec{k}}) \tag{1.16}$$

Now, we can use equation 1.7 to find $dE^0_{\vec{k}}/dk$:

$$\left| \frac{dE^0_{\vec{k}}}{dk} \right| = \frac{\hbar^2 |k|}{m_0} \tag{1.17}$$

With this substitution, equation 1.16 becomes

$$D_{2D}(E) = \frac{m_0}{\pi\hbar^2} \int_0^\infty dE^0_{\vec{k}}\, \delta(E - E^0_{\vec{k}}) \tag{1.18}$$

The integral evaluates to 1, leaving

$$D_{2D}(E) = \frac{m_0}{\pi\hbar^2} \tag{1.19}$$

The result that the two-dimensional density of states is constant will make the math of filling the energy subbands of the quantum wells very easy.

1.2.2 Single Band Method

Solving the Schrödinger Equation in One Dimension

The problem of finding the electron energies and wavefunctions in a quantum well or series of quantum wells is simplified by using separation of variables. We will assume that the electrons in the plane of the well act as a 2-dimensional electron gas as described in the previous section, thus allowing us to solve the system completely by just finding the energies and wavefunctions in the quantum confined direction.

Define the quantum well to be confining electrons along the z-axis. That is, the potential produced by the conduction band offset between LAO and

STO is a function $V_{BG}(z)$ that I will refer to as the background potential. The Schrödinger Equation for the confined energy levels is

$$\hat{H}\phi(z) = \left[-\frac{\hbar^2}{2m^*}\frac{d^2}{dz^2} + V_{BG}(z)\right]\phi(z) = E_z\phi(z) \tag{1.20}$$

Here m^* is the effective mass of the electron. The effective mass originates due to the band structure of STO. For this work, it will suffice to imagine that any electron in STO will act as though its mass is m^* instead of m_0; the m_0 in previously defined equations will be replaced by m^* in the context of electrons traveling within a solid.

We will employ the finite difference approximation to transform equation 1.20 to a form that can be solved numerically. This method takes the first and second order terms of the Taylor series for ϕ and rearranges them to solve for derivatives of ϕ:

$$\frac{d}{dz}\phi(z_0) \approx \frac{\phi(z_0+\Delta) - \phi(z_0-\Delta)}{2\Delta} \tag{1.21}$$

$$\frac{d^2}{dz^2}\phi(z_0) \approx \frac{\phi(z_0+\Delta) - 2\phi(z_0) + \phi(z_0-\Delta)}{\Delta^2} \tag{1.22}$$

These approximations approach equality as Δ goes to 0. Now, if we define a grid so that $z_m = m\Delta$ and $\phi_m = \phi(z_m)$, we can acquire:

$$\frac{d^2}{dz^2}\phi_m = \frac{1}{\Delta^2}(\phi_{m+1} - 2\phi_m + \phi_{m-1}) \tag{1.23}$$

Letting ϕ be a vector with m-th element ϕ_m and $V_m = V_{BG}(z_m)$, equation 1.23 transforms equation 1.20 into the following system of linear equations:

$$\hat{H}\phi_m = E_z\phi_m \tag{1.24}$$

$$\hat{H} = \frac{\hbar^2}{2m^*\Delta^2}\begin{pmatrix} 2 & -1 & 0 & \cdots & 0 \\ -1 & 2 & -1 & \cdots & 0 \\ 0 & -1 & 2 & \cdots & 0 \\ \vdots & \vdots & \vdots & \ddots & \vdots \\ 0 & 0 & 0 & \cdots & 2 \end{pmatrix} + \begin{pmatrix} V_1 & 0 & 0 & \cdots & 0 \\ 0 & V_2 & 0 & \cdots & 0 \\ 0 & 0 & V_3 & \cdots & 0 \\ \vdots & \vdots & \vdots & \ddots & \vdots \\ 0 & 0 & 0 & \cdots & V_n \end{pmatrix} \tag{1.25}$$

Now what we have is an eigenvalue equation. The eigenvalues of $\hat{H}$ will approach the true solutions E_z as Δ goes to 0 and n becomes large. Additionally, the eigenvectors ϕ will approximate the wavefunctions for each energy level.

Doping and Band Filling

Now that we have constructed the quantum confined wavefunctions, we can determine the electron distribution in the conduction band according to [8]. The conduction band is populated through doping. In a heterostructure, STO layers can be doped with Lanthanum. This means some of the Sr atoms are replaced with La atoms. The La atoms introduced into the system donate their valence electrons at a rate of 1 per atom according to the dopant density function $d(z)$. This function looks like a step function that takes on positive values within the STO layers and zero within the LAO layers.

Knowing the electron density and the quantum confined energy levels, we can determine the number of electrons in each energy level. We begin with the total energy of an electron in a quantum well:

$$E_{tot} = E_z + \frac{\hbar^2}{2m^*}(k_x^2 + k_y^2) \tag{1.26}$$

If we assume that an electron will settle into the lowest available total energy state, we can begin to use the density of states defined in section 1.2.1. We will begin by defining the Fermi energy, E_F as the energy of the highest occupied state. So, indexing the z-energy levels by i, each level also has an associated Fermi wavevector $\vec{k}_{F,i}$ in the xy plane according to:

$$E_F = E_{z,i} + \frac{\hbar^2}{2m^*}|\vec{k}_{F,i}|^2 \tag{1.27}$$

If E_F lies between $E_{z,n}$ and $E_{z,n+1}$, we can add equation 1.27 to itself n times, one for each occupied subband:

$$nE_F = \sum_i^n \left(E_{z,i} + \frac{\hbar^2}{2m^*}|\vec{k}_{F,i}|^2 \right) \tag{1.28}$$

Now, the area density of electrons in the well is the integral of $D_{\vec{k}}$ for $\vec{k}$ below the Fermi wavevector, summed over the subbands and done in polar

coordinates:

$$\begin{aligned}\frac{N}{A} &= \sum_i^n 2\pi \int_0^{k_F} dk\, D_{\vec{k}}\, k \\ \frac{N}{A} &= \frac{1}{\pi}\sum_i^n \int_0^{k_F} dk\, k \\ \frac{N}{A} &= \frac{1}{2\pi}\sum_i^n k_{F,i}^2\end{aligned} \tag{1.29}$$

We can substitute equation 1.29 back into equation 1.28 to obtain:

$$\begin{aligned}nE_F &= \frac{\pi\hbar^2}{m^*}\sigma_{2D} + \sum_i^n E_{z,i} \\ E_F &= \frac{\pi\hbar^2}{nm^*}\sigma_{2D} + \frac{1}{n}\sum_i^n E_{z,i}\end{aligned} \tag{1.30}$$

where σ_{2D} is the electron area density. This all leads to a simple expression for the area density of electrons occupying a give z subband. Returning to equations 1.29 and 1.27, we obtain

$$\sigma_{2D,i} = \frac{k_{F,i}^2}{2\pi} = \frac{m^*}{\pi\hbar^2}(E_F - E_{z,i}) \tag{1.31}$$

Charge Distribution and the Poisson Equation

Now that we know how many electrons go into each z-subband, we can find a charge distribution. According to Poisson's equation, this will then lead to an effective electron potential:

$$\frac{\partial^2}{\partial z^2} V_{\text{eff}}(z) = \rho(z) \tag{1.32}$$

Here $\rho(z)$ is the volume charge density in the material. We assume that the doping density and the electron density are constant in the xy plane, so the function only depends on position relative to the quantum well. To find $\rho(z)$, we assume the electrons and positive ions contributed by STO are evenly spread out in the quantum well, so that the only charge density comes from the dopant atoms and their electrons. The dopant atoms will

distribute the charge in the well according to $d(z)$ and the electrons will be located according to

$$\sigma_{2D}(z) = \sum_{i}^{n} \sigma_{2D,i} |\phi_i(z)|^2 \tag{1.33}$$

The charge distribution in the well is then just the sum of that from the La^+ ions and the negative donor electrons:

$$\rho(z) = d(z) - \sigma_{2D}(z) \tag{1.34}$$

Using this charge density, the effective electron potential is found simply by integrating twice over the z_i. The resulting magnitude of V_{eff} is usually on the order of $V_{BG} \cdot 10^{-3}$, so integration by adding trapezoidal subregions is sufficient to move on to the next step.

Self-Consistent Iterative Solution

Now we have a new classical potential representing the interactions between an electron and the other charges in the quantum well. So, we can take this potential and put it back into the Schrödinger Equation in the form

$$V^{(i+1)} = V_{BG}^{(i)} + V_{\text{eff}}^{(i)} \tag{1.35}$$

We continue to solve for new potentials until the ground state energy from iteration $(i+1)$ has converged to the ground state energy from iteration (i). The tolerance for this convergence is on the order of 10^{-7}[8].

1.2.3 Energy Transitions

Now that we have the electron wavefunctions in the quantum well, we wish to find the probability that an electron can jump up to a new energy state upon stimulation by a photon. This will allow us to calculate absorption spectra for doped wells and assess the ability of a given structure to produce energy transitions like those needed for lasers and sensing devices. For this calculation, we assume a very simplified picture of the real system: temperature is absolute zero and there are only enough electrons in the well to fill the ground state. Then, we only consider the transition $1 \rightarrow 2$, which will produce the largest absorption peak. After Helm [9], we first define the

oscillator strength, $f_{nn'}$, of a transition between states n and n':

$$\begin{aligned} f_{nn'} &\equiv \frac{2m^*\omega_{n'n}}{\hbar}|z_{nn'}|^2 \\ \omega_{nn'} &\equiv \frac{E_{n'} - E_n}{\hbar} \\ z_{nn'} &\equiv \int_{-\infty}^{\infty} dz\, \phi_n(z)\, z\, \phi_{n'}(z) \end{aligned} \tag{1.36}$$

Later in the results, the values of $z_{nn'}$ are listed for some transitions. This is called the transition dipole between the two states, and can be thought of as a measure of how likely an electron is to jump between the states when hit with a photon of the same energy as the energy difference between the two states. Helm [9] goes further to derive the absorption coefficient α_{2D} from these definitions. This coefficient is the ratio of absorbed electromagnetic energy per unit time per unit area per unit intensity of incident radiation. This gives a measure of the electromagnetic energy absorbed by a quantum well per unit cross-sectional area:

$$\alpha_{2D} = \frac{n_s e^2 \hbar}{2\epsilon_0 c \eta m^*} f_{12} \frac{\Gamma}{(E_2 - E_1 - \hbar\omega)^2 + \Gamma^2} \tag{1.37}$$

where n_s is the area density of electrons, e is the electron charge, c is the speed of light, η is the refractive index (about 2.6 for STO), Γ is the linewidth of the incoming radiation, and $\hbar\omega$ is the energy of the incoming radiation. This α_{2D} is dimensionless; normally we speak of α being the absorption coefficient in units of inverse length. To obtain the usual absorption coefficient α for a multiple quantum well structure, we simply divide α_{2D} by the period length of the structure and multiply by the number of periods.

Chapter 2

Results

2.1 The Code

These results were all calculated using various functions and scripts from the MATLAB library "PSsolver" (standing for "Poisson-Schrödinger solver"), which I have written from scratch during the course of this work. The workflow of the code begins by reading a parameter file and creating arrays over a discretized domain for the various functions (background potential, effective mass, etc.). It then generates a Hamiltonian and diagonalizes it using MATLAB's eig and eigs functions. All other operations (like finding inner products, and plotting) are performed relatively simply by the native vectorization scheme.

2.2 Convergence Analysis

First we will compare the energy levels to those we know from analytical results. The energy levels from an infinite quantum well are given by

$$E_n = \frac{\hbar^2 \pi^2 n^2}{2 m_0 L^2} \tag{2.1}$$

where L is the well width. These are plotted in Figure 2.1. The code slightly undershoots the analytical energy levels; the error between the analytical energy levels and the calculated levels is given in Figure 2.2, with the absolute error given by

$$\delta = \frac{|E_{calculated} - E_{analytical}|}{E_{analytical}} \tag{2.2}$$

In a finite quantum well we see a similar trend for energy versus the well

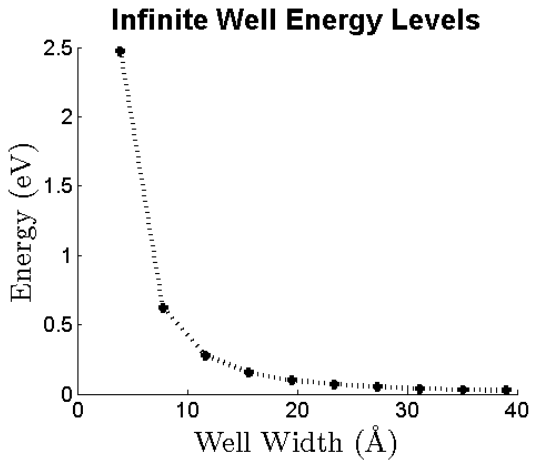

Figure 2.1: The relationship between ground state energy and well width for an infinite quantum well

width. This time, however, there is no analytical expression for the energy. Instead, the energy levels for a $2.4\,V$ finite well are the solutions of

$$\begin{aligned} k &= \sqrt{\frac{2m^*E}{\hbar^2}} \\ \kappa &= \sqrt{\frac{2m_0(2.4-E)}{\hbar^2}} \\ 0 &= \cos(kL) + \left(\frac{m^*\kappa}{m_0 k} - \frac{m_0 k}{m^*\kappa}\right)\sin(kL) \end{aligned} \tag{2.3}$$

m^* is the effective mass inside the well and this assumes the effective mass is m_0 outside the well. This also has to be done numerically, but this result will get us arbitrarily close to the true energy levels. These energy levels are plotted in Figure 2.3, and the convergence is shown in Figure 2.4.

2.3 Single-Band Calculations

The single band calculations can show where the charge density is likely to be localized and if there will be any mixing in wells separated by thin barriers.

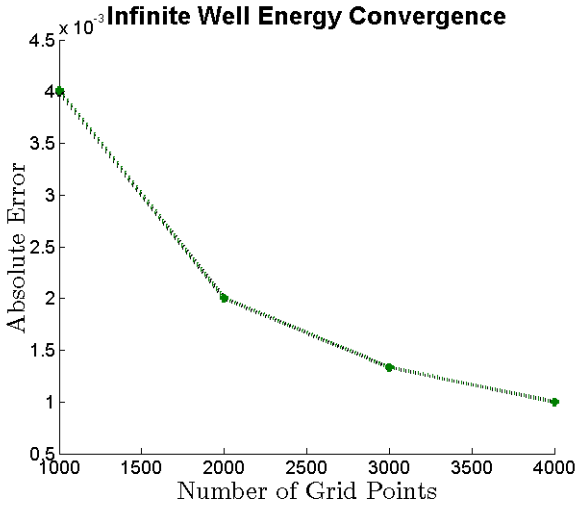

Figure 2.2: The convergence of the ground state of a 5 unit cell infinite quantum well

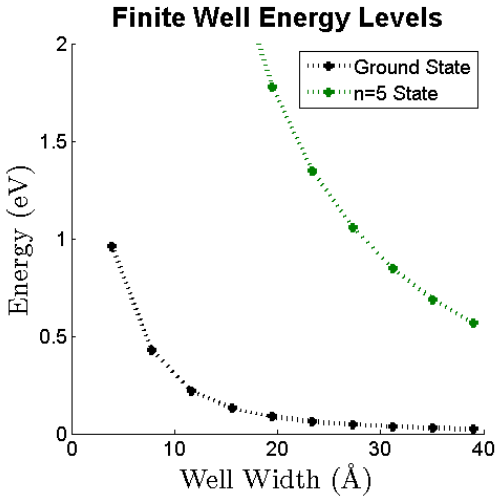

Figure 2.3: The relationship between energy and well width for a finite quantum well

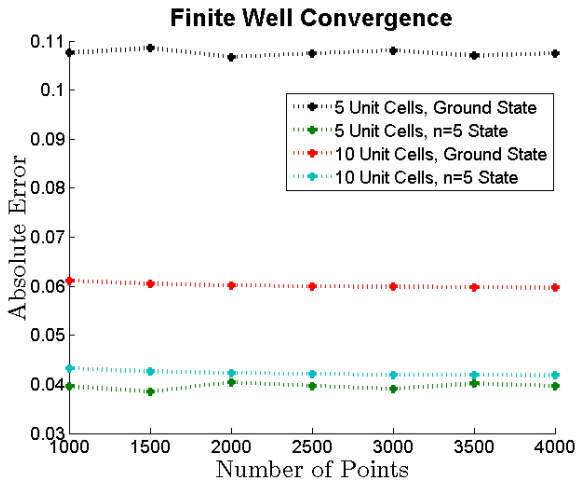

Figure 2.4: Convergence for various finite quantum wells, all of height $2.4\,V$

It can also give an estimate of the expected transitions available in a given sample. Some examples of these different uses are shown.

Figure 2.5 shows the wavefunctions for a single 5 unit cell quantum well. These energy levels will differ slightly for different effective masses. Figure 2.6 shows two quantum wells placed with a thin (1 unit cell) barrier between them, which shows that the electrons can tunnel through a barrier if it is thin enough. The well on the right side is raised by the effective electron potential after they migrate to the lowest available energy state.

2.4 Absorption Spectra and Energy Transitions

When wavefunctions are known, we can calculate optical properties of the wells. Figure 2.7 shows the absorption spectrum for a multiple quantum well (MQW) structure, designed to increase the signal in experiments beyond that of a single quantum well structure. There are other transitions at higher energies that don't appear because they are orders of magnitude smaller. Figure 2.8 shows the same calculation for a different structure for

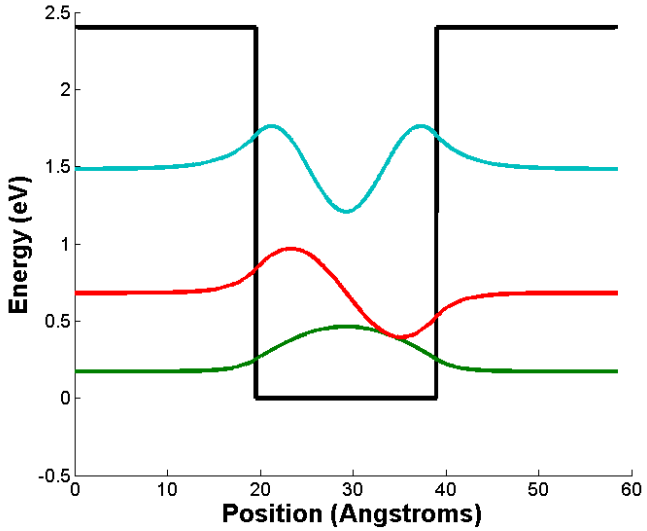

Figure 2.5: The wavefunctions for a single LAO/STO quantum well structure with $m^* = .39m_0$. The y-intercepts represent the energy levels

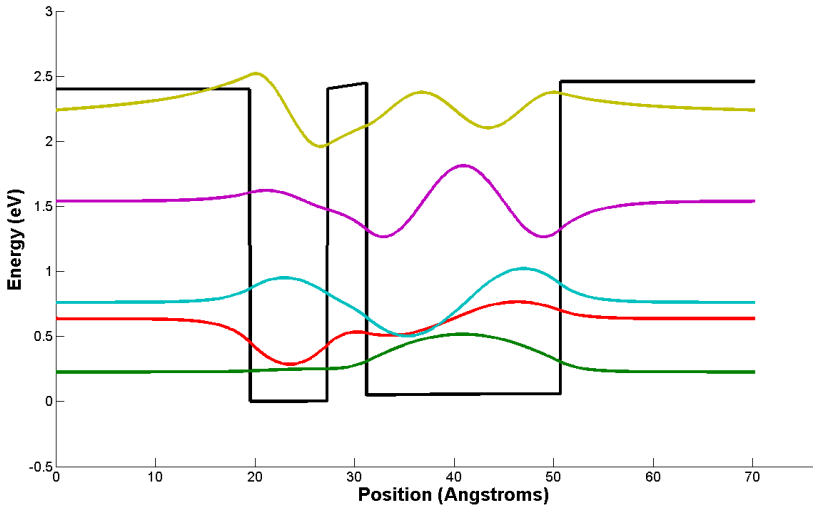

Figure 2.6: The wavefunctions in a coupled quantum well exhibit mixing when the barrier is thin

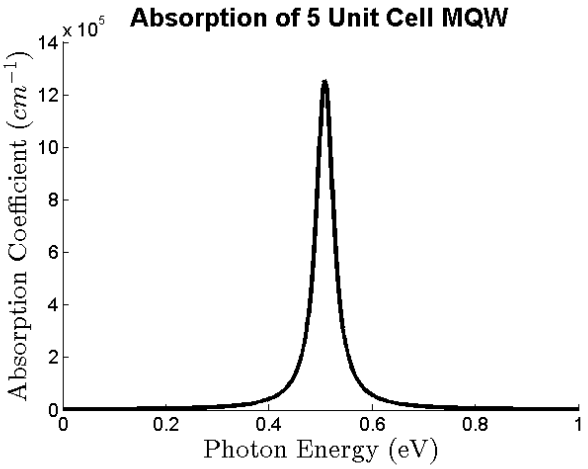

Figure 2.7: The absorption spectrum of a periodic quantum well structure with a 5 unit cell well followed by a 7 unit cell barrier, repeated 20 times

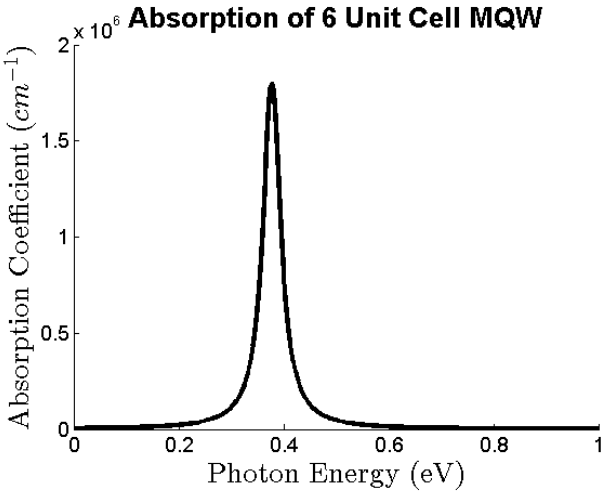

Figure 2.8: The absorption spectrum of a periodic quantum well structure with a 6 unit cell well followed by a 4 unit cell barrier, repeated 20 times

comparison. The only real difference is a shift in energy and a slight change in the magnitude of the absorption coefficient that comes from the size of the structure.

Figure 2.9 shows the wavefunction moduli and their transition dipoles for a biased double well with a 1 unit cell barrier. This sample has a bias voltage bending the bands; this serves to slightly shift the energy levels in the desired direction.

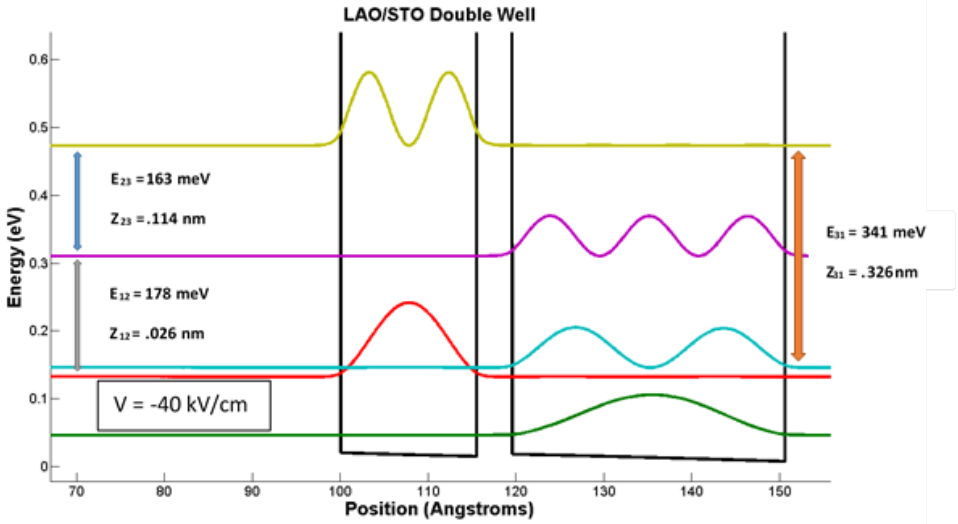

Figure 2.9: Some available transitions along with their quantum dipoles in a double well structure

Chapter 3

Discussion

3.1 Convergence and Sensitivity Analysis

To determine if any of the results from this code are worthwhile, first it is important to see how the results compare to known, analytical solutions to Schrödinger's Equation. We are also interested in how the energy levels change with changes in well width, well height, and well effective mass, because this can inform our sample synthesis for experiments even if the energies don't match the calculated values. It will be more convenient if these calculations turn out to match the experimental results, but we can still learn about different quantum wells by studying the trends and applying our newfound knowledge to future experiments.

First consider plots 2.1 and 2.3 that show the width dependence of the ground state energies for finite and infinite wells. At smaller widths the infinite well ground states are significantly higher than those of the finite well but at larger well widths the values begin to converge. We are mostly dealing with the lower energy levels of the quantum wells because those are typically the ones that are filled by doping. This is interesting because [10] actually models the LAO/STO quantum well as an infinite well based on arguments that the electrons have no bands to go to when moving into the LAO layer. So, experimental results will show whether the finite or infinite well approach is correct for the thin wells (1 - 4 unit cells), but as the wells get thicker both approaches should agree more closely.

For the convergence of the two calculations (plots 2.2 and 2.4) we see two slightly differing results. The infinite well convergence shows a smooth decrease in error as we increase the number of grid points allowed. At some point we have diminishing returns as the calculation time scales as n^2 while the error levels off. Luckily, since these calculations use a lot of approximations in the first place, we aren't expecting them to be within .001% of the experimental value. The trends and energy differences in the wells are much more important. The more interesting convergence plot is the one for the finite well calculation (Figure 2.4). This plot shows no error dependence on the number of grid points used, and no suggestion of how to decrease the error inherent in using the finite difference method. The root finder to get the "analytical" energy levels is continuous, so the error from that is negligible on this scale. The main takeaway from this convergence plot is the higher energies and wider wells produce slightly more accurate calculations.

3.2 Single Band Calculations

In this context, any single calculation will not mean much on its own, but the ability to find the energy levels before a structure is synthesized could potentially save a significant amount of time and money when designing experiments. So, we consider just a couple of example structures with the knowledge that we can produce the same information on any other structure.

The first plot (Figure 2.5) shows a simple, single quantum well structure. This is the basic building block for all of the other structures we wish to study. Ultimately, these energies will be tested/verified with photoemission spectroscopy to see if the calculations are correct and update the model to give more predictive power for future experiments.

The second plot (Figure 2.6) shows a HEMT-like structure as described in Section 1.1. We can find the wavefunctions for much more complex multiple quantum well structures like this by employing the same calculation that was described for the single well, except with a more complex background potential. In the figure, the electrons are shown to migrate across the thin LAO barrier because there is a lower energy state available in the larger well. In this way, the code could also solve for the wavefunctions in a quantum cascade laser, choosing the well and barrier widths to give desired energy

transitions for lasing. This illustrates the flexibility afforded by using the large-bandgap materials: the wells are taller so there are more possibilities for larger transitions than in a semiconductor well.

3.3 Absorption Spectra and Energy Transitions

Energy transition data are the ultimate goal of the ongoing experimental studies. With applications for lasing and sensing, the goal of the calculations is to provide parameters for promising energy transitions. So, we require absorption spectra and measures of transition probabilities between states, in addition to the allowed energy shifts.

Once we have used the Schrödinger - Poisson solver to find the energies and wavefunctions within a heterostructure, we can employ the math from Section 1.2.3 on Energy Transitions to find the quantum dipoles and the absorption spectra of that heterostructure. Figures 2.7 and 2.8 illustrate this ability. Both peaks correspond to the $n = 1$ to $n = 2$ transition, which is the largest contributor in these structures. The peak near .5 eV for the 5 unit cell well corresponds to a frequency of about 120 THz, which is right in the middle of the infrared region of the electromagnetic spectrum with potential uses in communication technology. The absorption coefficient itself is not particularly high but should be enough to see in upcoming experiments on the structure.

Figure 2.9 illustrates the type of calculation that is being used to find well sizes for certain energy transitions. Here, two coupled wells have been shifted by a bias voltage to give two approximately equal energy steps. This specific structure is not being used currently but others like it are being synthesized for absorption and emission studies. This is an illustration of how adjusting well widths can lead to control over the available energy transitions.

3.4 Future Directions

The $k \cdot p$ perturbation theory used in [10] would be the most obvious next step. This would allow us to find energy levels while incorporating the band

structure of STO and LAO beyond just using a constant effective mass. We could also consider the interactions between bands and simultaneously use the different effective masses that arise from bands originating as different atomic orbital states. There are also other methods for calculating the energy eigenvalues like the transfer matrix approach outlined in [8] that could give more accurate energies than the finite difference method. These methods could be used to design infrared lasers and signal sensing devices.

The experimental studies for these and other LAO/STO heterostructures are currently ongoing with results pending. This data and other data generated by the code will also be used to come up with more heterostructures that are worth studying, specifically trying to design materials with better absorption, transitions, and specific energies in the infrared region of the spectrum.

Chapter 4

Acknowledgements

First and foremost I would like to thank Alex Demkov. For the past two years he has given me a home in his research group, answered my dumb physics questions, written recommendations, and assisted me in life decisions like where to attend graduate school. I could not have achieved anything significant in the past two years if not for his help, and for that I am overflowing with gratitude. I have also had help from others along the way. Mark Sholte spent a good portion of my first year in the group walking me through writing my first computer program outside of an introductory CS course, and he played a major role in getting the project off the ground. Elliott Ortmann has created the structures I have calculated and is hard at work on the ongoing experiments, so without him I would have run out of things to calculate. Last but not least, I would like to thank Mikhail Belkin for working with us on an upcoming project studying the response of LAO/STO MQWs when exposed to light.

This project also happened with the help of some sponsors. I would like to thank both the Semiconductor Research Corporation and Schlumberger for providing me with funding during the past year and a half. Their support allowed me to spend much more time working on this project than I would have been able to otherwise.

Bibliography

[1] Charles Kittel. *Introduction to Solid State Physics*. Wiley, 8 edition, 2004.

[2] A. Ohtomo and H. Y. Hwang. A high-mobility electron gas at the $LaAlO_3/SrTiO_3$ heterointerface. *Nature*, 427(6973):423–426, 01 2004.

[3] Berner et al. Band alignment in $laalo_3/srtio_3$ oxide heterostructures inferred from hard x-ray photoelectron spectroscopy. *Phys. Rev. B*, 88(11), 9 2013.

[4] C. Jirauschek and T. Kubis. Modeling techniques for quantum cascade lasers. *Appl. Phys. Rev.*, 1(1), 2014.

[5] Masayoshi Tonouchi. Cutting-edge terahertz technology. *Nature Photonics*, 1:97–105, 2007.

[6] Michael P. Marder. *Condensed Matter Physics*. Wiley, 2 edition, June 2010.

[7] et al. Cheng. An integrated approach for structural characterization of complex solid state electrolytes: the case of lithium lanthanum titanate. *Journal of Mat. Chem. A*, 2(7), 2014.

[8] Paul Harrison. *Quantum Wells, Wires and Dots: Theoretical and Computational Physics of Semiconductor Nanostructures*. Wiley, 3 edition, September 2011.

[9] Manfred Helm. *Intersubband Transitions in Quantum Wells: Physics and Device Applications I*, volume 62 of *Semiconductors and Semimetals*. Academic Press, 2000.

[10] L. van Heeringen. The band structure of $SrTiO_3/LaAlO_3$ heterostructures. diploma thesis, Radboud University Nijmegen, 2012.